

Unsupervised Deep Graph Matching Based on Discrete Cycle Consistency

Siddharth Tourani*

tourani.siddharth@gmail.com

Carsten Rother*

carsten.rother@iwr.uni-heidelberg.de

Muhammad Haris Khan†

muhammad.haris@mbzuai.ac.ae

Bogdan Savchynskyy*

bogdan.savchynskyy@iwr.uni-heidelberg.de

Abstract

We contribute to the sparsely populated area of unsupervised deep graph matching with application to keypoint matching in images. Contrary to the standard supervised approach, our method does not require ground truth correspondences between keypoint pairs. Instead, it is self-supervised by enforcing consistency of matchings between images of the same object category. As the matching and the consistency loss are discrete, their derivatives cannot be straightforwardly used for learning. We address this issue in a principled way by building our method upon the recent results on black-box differentiation of combinatorial solvers. This makes our method exceptionally flexible, as it is compatible with arbitrary network architectures and combinatorial solvers. Our experimental evaluation suggests that our technique sets a new state-of-the-art for unsupervised graph matching.

1. Introduction

Graph matching (GM) is an important research topic in machine learning, computer vision and related areas. It aims at finding an optimal node correspondence between graph-structured data. It can be applied in tasks like shape matching [28], activity recognition [4], social network analysis [42], point cloud registration [15] and many others. One classical application of graph matching also considered in our work is keypoint matching, as illustrated in Fig. 1.

A modern learning-based approach to this problem tries to estimate costs for the subsequent combinatorial matching algorithm. The learning is usually supervised, *i.e.*, ground truth correspondences are given as training data. However, obtaining ground truth is costly, which motivates development of unsupervised learning methods.

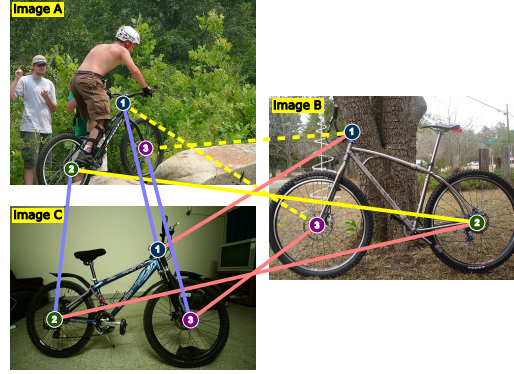


Figure 1: Illustration of cycle consistency in multi-graph matching (best viewed in color). There are three nodes in each image. They are labelled by both color (blue, green, purple) and numbers (1, 2, 3). Matches between pairs of nodes are shown by colored lines. $A \leftrightarrow B$, $B \leftrightarrow C$ and $C \leftrightarrow A$ are color coded with yellow, light purple and light pink lines. Correct matches are shown by solid, wrong matches by dotted lines. Matching of the node 2 is cycle consistent across the images, whereas nodes 1 and 3 are not.

Our work proposes one such unsupervised technique. Instead of ground truth correspondences, our method utilizes the *cycle consistency* constraint as a supervision signal, see Fig. 1. Based on pairwise correspondences of multiple images, we iteratively update matching costs to improve consistency of the correspondences.

1.1. Related work

Supervised deep graph matching methods typically consist of two parts: *Feature extraction* and *combinatorial optimization*. Whereas the first part is nowadays carried out by neural networks, the second is responsible for finding a one-to-one, possibly incomplete, matching. As it is shown in [33, 1], neural networks do not generalize on combinatorial tasks and cannot substitute combinatorial methods therefore.

*Computer Vision & Learning Lab, University of Heidelberg

†MBZUAI

The **architecture of the neural networks** of recent deep graph matching methods such as [27] or [35] is very similar. As a backbone they use a VGG16 [19] or similar convolutional network for visual feature generation and a graph neural network for their refinement and combination with the geometric information. Apart from specific parameters of the used networks, the key differences are the type of combinatorial solvers they use and the way they deal with differentiation through these solvers.

A number of **combinatorial techniques** have been proposed to address the matching problem itself, see the recent benchmark [16] and references therein. One distinguishes between linear and quadratic formulations, closely related to the *linear and quadratic assignment problems* (LAP and QAP resp.). These are deeply studied in the operations research [5]. Whereas the optimal linear assignment minimizes the sum of node-to-node (cf. keypoint-to-keypoint in Fig. 1) matching costs, the quadratic assignment penalizes pairs of nodes (pairs of keypoints) matched to each other. Most importantly, this allows to take into account relative positions of the respective keypoints.

The greater expressive power of QAPs comes at a price: In general this problem is NP-hard, whereas LAP can be exactly and efficiently solved with a number of polynomial algorithms, see a practical analysis in [8]. Most learning pipelines, however, adopt an approximate LAP solver based on the *Sinkhorn normalization (SN)* [3, 26] due to its inherent differentiability [11].

Despite the computational difficulty of QAPs, best existing algorithms are able to provide high-quality approximate solutions for problems with hundreds of keypoint within one second or even less [16]. This speed allows their direct use in end-to-end training pipelines provided there exists a way to differentiate through the solvers.

The differentiability issue. When incorporating a combinatorial solver into a neural network, differentiability constitutes the principal difficulty. Such solvers take continuous inputs (matching costs in our case) and return a discrete output (an indicator vector of an optimal matching). This mapping is piecewise constant because a small change of the costs typically does not affect the optimal matching. Therefore, the gradient exists almost everywhere but is equal to zero. This prohibits any gradient-based optimization.

The need for end-to-end differentiability has given rise to various approaches that utilize differentiable relaxations of combinatorial optimization techniques [25, 41, 18, 36, 40, 13, 35]. At the end of their pipeline, all these methods use the Sinkhorn normalization. *However, such methods are either limited to approximately solving the LAP, or are solver specific, when addressing the QAP.*

The most general technique providing a *black-box differentiation of combinatorial solvers* was recently proposed in [33]. Applied to deep graph matching [27] it is still the

state-of-the art method in this domain. *We also make use of this technique in our work.*

Multi-graph matching (MGM) is a generalization of graph matching for computing correspondences between *multiple* images of the same object. From an optimization point of view, the goal is to minimize the total matching cost between all pairs of such images given the *cycle consistency* of the matchings [29]. No exact polynomial algorithm is known for this problem even if matching of each two objects is formulated as LAP. Apart from optimization, recent works in this domain include also learning of the matching costs, see, e.g., [35]. *Contrary to these works, we do not enforce cycle consistency during inference, and only use it as a supervision signal for training.*

Unsupervised deep graph matching. The field of unsupervised deep graph matching is still under-studied. Essentially, it contains two works. The *first* one [34], referred to as GANN, uses cycle-consistent output of an MGM solver as pseudo-ground truth for training a differentiable QAP-based matching. Costs involved in MGM as well as the QAP are updated during training, to make the output of both algorithms closer to each other in the sense of a *cross-entropy* loss. The method is restricted to specific differentiable algorithms and biased to the sub-optimal solutions provided by the used MGM solver.

The *second* unsupervised training technique called SCGM [23] is based on contrastive learning with data augmentation. Specifically, in the unsupervised training stage each image and the respective keypoint graph is matched to its artificially modified copies. The known mapping between original and modified keypoint graphs serves as ground truth. This technique can be applied with virtually any deep graph matching method as a backbone. Nothing prevents it from being used as a pre-training for our method.

However, a well-performing data augmentation usually requires significant fine-tuning to match the actual unknown data distribution. Additionally, SCGM uses two views of the same image to build its graph matching problem. It is thus biased towards complete matchings, which is a disadvantage in real world matching scenarios.

Cycle consistency has been used in various computer vision applications as a supervision signal to train correspondences in videos, e.g., [36] or dense semantic matching [20]. However, in these works only a pair A, B of matched objects is considered and consistency of the direct $A \rightarrow B$ and the inverse $B \rightarrow A$ mappings is enforced. Alternatively, the seminal work [43] leverages synthetic (3d CAD) objects to obtain correct (2d image-to-image) correspondences, which is rarely possible.

In contrast, we treat the cycle consistency of *each subset*

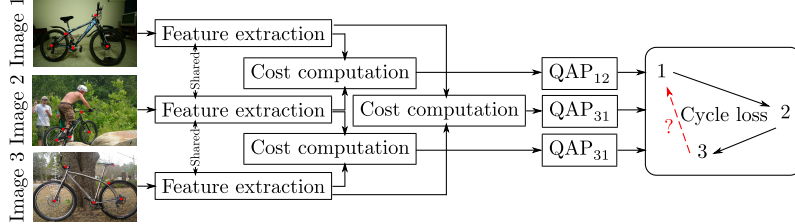


Figure 2: Overview of our framework for a batch of 3 images. Features extracted from images and keypoint positions are transformed into matching costs for each pair of images. The resulting integer linear program **ILP** block computes the matchings either as LAP or QAP. At the end the **cycle loss** counts a number of inconsistent cycles and computes a gradient for back propagation.

of the matched graphs as a supervision signal. This is opposed to merely considering direct-and-inverse consistency, as the latter does not entail general cycle consistency.

The recent work on unsupervised shape matching learning [6] enforces cycle consistency in a principally different way than we do, by leveraging the powerful functional map regularisation on the model of the universe shape. Although very promising, this approach requires a restrictive model and therefore is hardly applicable to general graph matching and in our application in particular.

1.2. Contribution

- We present a new principled framework for unsupervised end-to-end training of graph matching methods. It is based on a *discrete* cycle loss as a supervision signal and the black-box differentiation technique for combinatorial solvers [33].
- *Arbitrary* network architectures as well as *arbitrary* combinatorial solvers addressing LAP or QAP problems can be used within our framework. It can handle incomplete matchings if the respective solver can.
- We also contribute a novel architecture combining Spline CNNs and cross-attention layer to aggregate information across graphs to improve feature expressivity for deep graph matching.

An extensive empirical evaluation suggests that our method sets a new state-of-the-art for unsupervised graph matching. Our code will be made public upon acceptance.

2. Overview of the proposed framework

Figure 2 provides an overview of our architecture. First the features are computed for each keypoint in each image (block **Feature extraction**). These features are translated to matching costs for each pair of images (block **Cost computation**) and the respective optimization QAP or LAP problems (blocks **QAP**₁₂, **QAP**₂₃, **QAP**₃₁) are solved. Finally, **cycle loss** computes the *number of inconsistent cycles*.

We address all components one by one:

- Section 3 overviews the black-box differentiation technique [33] that addresses the differentiability question

discussed in Section 1. As the method requires a combinatorial solver to be represented in the integer linear program format, we briefly introduce this representation for LAP and QAP problems.

- Section 4 describes the key contribution of our work - the cycle consistency loss and its differentiation.
- Section 5 describes the feature extraction and cost computation networks.

Finally, our experimental validation is given in Section 6. More detailed results are available in the supplementary.

3. Background

Black-box differentiation of combinatorial solvers. The work [33] overcomes the zero gradient problem for discrete functions in a principled way. It introduces efficient piecewise-linear approximations of the considered piecewise constant objective functions. This has the effect of making the gradient of the approximated function informative, thus allowing for gradient-based training. Let $\mathbf{c} \in \mathbb{R}^n$ be continuous input costs and $\mathbf{x} \in \mathcal{X}$ be a discrete output taken from an arbitrary finite set \mathcal{X} . An important property of the method [33] is that it allows to use *arbitrary* combinatorial solvers as a *black-box*, as soon as the costs \mathbf{c} and the output \mathbf{x} are related via an *integer linear program* (ILP):

$$\mathbf{x}(\mathbf{c}) = \arg \min_{\mathbf{x} \in \mathcal{X}} \langle \mathbf{c}, \mathbf{x} \rangle. \quad (1)$$

This general formulation covers a significant portion of combinatorial problems including LAPs and QAPs.

The flexibility of the black-box technique comes at the price of a somewhat higher computational cost. The used combinatorial solver must be run twice on each learning iteration: In addition to the normal execution on the forward pass, the backward pass involves another call to the solver with specially perturbed costs.

Essentially, if $L: \mathcal{X} \rightarrow \mathbb{R}$ denotes the final loss of the network, its gradient w.r.t. the costs \mathbf{c} can be approximated as

$$\frac{dL(\mathbf{x}(\mathbf{c}))}{d\mathbf{c}} := \frac{\mathbf{x}(\mathbf{c}^\lambda) - \mathbf{x}(\mathbf{c})}{\lambda}. \quad (2)$$

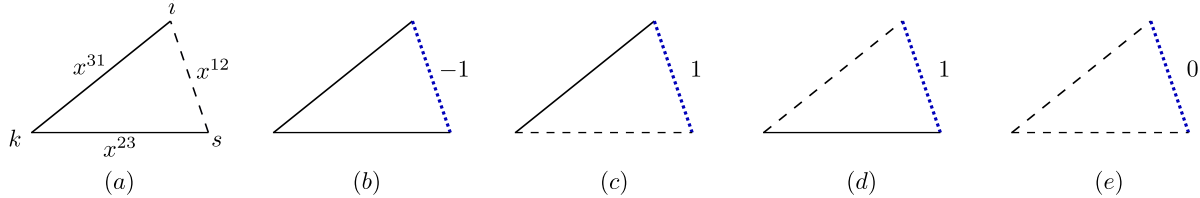


Figure 3: (a) Partial loss illustration for a triple of indices i, s, k and the respective binary variables x^{12}, x^{23}, x^{31} . The solid lines for x^{23} and x^{31} denote that these variables are equal to 1 and correspond to an actual matching between the respective points. The dashed line for x^{12} denotes that this variable is equal to 0 and therefore points indexed by i and s are *not* matched to each other. Given the values of x^{23} and x^{31} this violates cycle consistency. (b-e) Illustration of the values of the derivative $\partial\ell/\partial x^{12}$. The meaning of the solid and dashed lines as well as the position of x^{12}, x^{23} and x^{31} are the same as in (a). The thick blue dotted lines mean that x^{12} can be either 0 or 1, since $\partial\ell/\partial x^{12}$ does not depend on x^{12} value, see (8). So, for instance, $\partial\ell/\partial x^{12} = 1$ for $x^{23} = 0$ and $x^{31} = 1$ as illustrated by (c).

Here \mathbf{c}^λ is a *perturbed cost vector* computed as

$$\mathbf{c}^\lambda = \mathbf{c} + \lambda \frac{dL}{d\mathbf{x}}(\mathbf{x}(\mathbf{c})). \quad (3)$$

More precisely, Eq. (2) defines the gradient of a piecewise linear interpolation of L at $\mathbf{x}(\mathbf{c})$ with a hyperparameter $\lambda > 0$ controlling the interpolation accuracy. Equation (3) suggests that the loss function L is differentiable. Note that for the gradient computation (2) no explicit description of the set \mathcal{X} is required.

Graph matching problem (QAP and LAP). For our description of the graph matching problem we mostly follow [16]. Let \mathcal{V}^1 and \mathcal{V}^2 be two finite sets to be matched, *e.g.*, the sets of keypoints of two images. For each pair $i, j \in \mathcal{V}^1$, and each pair $s, l \in \mathcal{V}^2$, a cost $c_{is,jl}$ is given. Each such pair can be thought of as an edge between pairs of nodes of an underlying graph. In general, these costs are referred to as *pairwise* or *edge costs*. The *unary*, or *node-to-node* matching costs are defined by the diagonal terms of the *cost matrix* $C = (c_{is,jl})$, *i.e.*, $c_{is,ii}$ is the cost for matching the node $i \in \mathcal{V}^1$ to the node $s \in \mathcal{V}^2$. For the sake of notation we further denote it as c_{is} . In turn, is will stand for (i, s) below.

The goal of graph matching is to find a matching between elements of the sets \mathcal{V}^1 and \mathcal{V}^2 that minimizes the total cost over all pairs of assignments. It is represented as the following integer quadratic problem:

$$\min_{\mathbf{x} \in \{0,1\}^{\mathcal{V}^1 \times \mathcal{V}^2}} \sum_{is \in \mathcal{V}^1 \times \mathcal{V}^2} c_{is} x_{is} + \sum_{\substack{is, jl \in \mathcal{V}^1 \times \mathcal{V}^2 \\ is \neq jl}} c_{is,jl} x_{is} x_{jl} \quad (4)$$

$$\text{s.t. } \begin{cases} \forall i \in \mathcal{V}^1: \sum_{s \in \mathcal{V}^2} x_{is} \leq 1, \\ \forall s \in \mathcal{V}^2: \sum_{i \in \mathcal{V}^1} x_{is} \leq 1. \end{cases} \quad (5)$$

The *uniqueness constraints* (5) specify that each node of the first graph can be assigned to *at most one* node of the second graph. Due to inequality in these constraints one speaks about *incomplete* matchings contrary to the equality case termed as *complete*. The incomplete matching is

much more natural for computer vision applications as it allows to account for noisy or occluded keypoints. From the computational point of view both problem variants are polynomially reducible to each other, *see, e.g.*, [16] for details. Therefore we treat them equally unless specified otherwise.

By ignoring the second, quadratic term in (4) one obtains the LAP. Note that it already has the form (1) required for black-box differentiation. As for the more general QAP case, the substitution $y_{is,jl} = x_{is}x_{jl}$ linearizes the objective of (4) and makes it amenable to black-box differentiation. The resulting ILP problem with different linearizations of the substitution $y_{is,jl} = x_{is}x_{jl}$ added as a constraint to the feasible set is addressed by a number of algorithms, *see, e.g.*, [16]. We mention here only two, which we use in our work: The LPMP solver [29] employed in the work [27], and the *fusion moves* solver [17] showing superior results in [16].

4. Cycle consistency loss and its derivative

Let us denote the fact that a point i is matched to a point s as $s \leftrightarrow i$. We call a mutual matching of d point sets $\mathcal{V}^1, \dots, \mathcal{V}^d$ *cycle-consistent*, if for any matching sequence of the form $s^{k_1} \leftrightarrow s^{k_2}, s^{k_2} \leftrightarrow s^{k_3}, \dots, s^{k_{m-1}} \leftrightarrow s^{k_m}$ it holds $s^{k_m} \leftrightarrow s^{k_1}$, where $k_i \in \{1, \dots, d\}$, $k_i < k_{i+1}$, $i = 1, \dots, m$.

It is well-known from the literature, *see, e.g.*, [29], the cycle consistency over arbitrary subsets of matched point sets is equivalent to the cycle consistency of *all triples*. We employ this in our pipeline, and define the cycle consistency loss for triples only.

Let us consider a matching of three sets $\mathcal{V}^1, \mathcal{V}^2$ and \mathcal{V}^3 . We define the total cycle loss as the sum of *partial* losses for all possible triples of points from these sets: $L(\mathbf{x}^{12}, \mathbf{x}^{23}, \mathbf{x}^{31}) = \sum_{i \in \mathcal{V}^1} \sum_{s \in \mathcal{V}^2} \sum_{k \in \mathcal{V}^3} \ell(x_{is}^{12}, x_{sk}^{23}, x_{ki}^{31})$. Here \mathbf{x}^{12} denotes a binary matching vector, *i.e.*, a vector that satisfies the uniqueness constraints (5) between \mathcal{V}^1 and \mathcal{V}^2 . Vectors \mathbf{x}^{23} and \mathbf{x}^{31} are defined analogously.

Algorithm 1 Unsupervised training algorithm

Given: Sets of keypoints to be matched $\mathbb{V} := \{\mathcal{V}^i, i \in \{1, \dots, d\}\}$; λ - the hyper-parameter from Section 3.

1. Randomly select 3 sets from \mathbb{V} . W.l.o.g. assume these are $\mathcal{V}^1, \mathcal{V}^2$ and \mathcal{V}^3 .
2. Infer costs $\mathbf{c}^{12}, \mathbf{c}^{23}, \mathbf{c}^{31}$ for the 3 QAPs corresponding to the pairs $(\mathcal{V}^1, \mathcal{V}^2), (\mathcal{V}^2, \mathcal{V}^3), (\mathcal{V}^3, \mathcal{V}^1)$.
3. Solve the QAPs and obtain the respective matchings $\mathbf{x}^{12}, \mathbf{x}^{23}, \mathbf{x}^{31}$, see Fig. 3.
4. Compute the perturbed costs $[\mathbf{c}^{12}]^\lambda, [\mathbf{c}^{23}]^\lambda$ and $[\mathbf{c}^{31}]^\lambda$ based on (3) and the loss gradient (8), e.g.:

$$[\mathbf{c}_{is}^{12}]^\lambda := \mathbf{c}_{is}^{12} + \lambda \frac{\partial L}{\partial \mathbf{x}_{is}^{12}}, \quad is \in \mathcal{V}^1 \times \mathcal{V}^2. \quad (6)$$

5. Compute the solutions $\mathbf{x}^{12}([\mathbf{c}^{12}]^\lambda), \mathbf{x}^{23}([\mathbf{c}^{23}]^\lambda)$ and $\mathbf{x}^{31}([\mathbf{c}^{31}]^\lambda)$ to the QAP problems (4) with the perturbed costs.
6. Compute the gradients via (2) and backpropagate the changes to the network weights.

Assume now that the triple of point indices $(i, s, k) \in \mathcal{V}^1 \times \mathcal{V}^2 \times \mathcal{V}^3$ is fixed. For the sake of notation we omit the lower indices and assume $x^{12} = x_{is}^{12}, x^{23} = x_{sk}^{23}, x^{31} = x_{ki}^{31}$ to be binary variables, see Fig. 3(a) for illustration.

The partial loss ℓ penalizes cycle inconsistent configurations as the one illustrated in Fig. 3(a). In particular, the partial loss is equal to 1, if $x^{12} = 0$ and $x^{23} = x^{31} = 1$. This can be achieved by, e.g., the following differentiable function

$$\begin{aligned} \ell(x^{12}, x^{23}, x^{31}) &= \\ (1 - x^{12})x^{23}x^{31} + (1 - x^{23})x^{12}x^{31} + (1 - x^{31})x^{12}x^{23} \\ &= x^{12}x^{23} + x^{23}x^{31} + x^{12}x^{31} - 3x^{12}x^{23}x^{31} \end{aligned} \quad (7)$$

where the three terms are necessary to make sure the loss function is symmetric.

The derivative of the partial loss ℓ w.r.t. x^{12} reads

$$\frac{\partial \ell}{\partial x^{12}} = x^{23} + x^{31} - 3x^{23}x^{31}, \quad (8)$$

and analogously for variables x^{23} and x^{31} .

Fig. 3(b-e) illustrate the values of the derivative for the four possible cases. The gradient of L is the sum of gradients of ℓ over all index triples.

Algorithm 1 summarizes our cycle-loss based unsupervised learning approach. Note that in Step 4 only unary costs c_{is} are perturbed, as the pairwise costs $c_{is,jl}$ are multiplied by the lifted variables $y_{is,jl}$ in the linearized QAP objective, and $\partial L / \partial \mathbf{y} = 0$.

5. Network architecture

5.1. Feature extraction

Fig. 4 shows the information flow from input, through the feature extraction block, to the construction of the matching instance. The weights for the VGG16, SplineCNN and cross attention layers are shared across images. Input to the feature extraction block are the

image-keypoint pairs. We denote them as $(\text{Im}^1, \text{KP}^1)$ and $(\text{Im}^2, \text{KP}^2)$.

The SplineCNN layers require the definition of a graph structure for the keypoints per image. The keypoints form the nodes of the graph. We use the Delaunay Triangulation [9] of the keypoint locations to define the edge structure of this graph. We refer to the graphs of Im^1 and Im^2 as $(\mathcal{V}^1, \mathcal{E}^1)$ and $(\mathcal{V}^2, \mathcal{E}^2)$, respectively. For the sake of notation, we denote an edge (i, j) in an edge set \mathcal{E} as ij .

Backbone architecture. Following the works of [27, 13, 36] we compute the outputs of the `relu4_2` and `relu5_1` operations of the VGG16 network [19] pre-trained on ImageNet [10]. The feature vector spatially corresponding to a particular keypoint is computed via bi-linear interpolation. The set of feature vectors thus obtained are denoted as $\mathbf{F}^1, \mathbf{F}^2$ in Fig. 4.

SplineCNN based feature refinement. The keypoint features extracted from the VGG16 network are subsequently refined via SplineCNN layers [14]. SplineCNNs have been shown to successfully improve feature quality in point-cloud [22] and other graph structure processing applications [32].

The VGG16 keypoint features ($\mathbf{F}^1, \mathbf{F}^2$ in Fig. 4) are input to the SplineCNN layers as node features. The input edge features to the SplineCNNs are defined as the relative coordinates of the associated vertices. We use two layers of SplineCNN with MAX aggregations.

The outputs of the SplineCNN layers are added to the original VGG node features to produce the refined node features, denoted as $\mathcal{F}^1, \mathcal{F}^2$. The edge features $\mathcal{P}^k, k = 1, 2$, are computed as $\mathcal{P}_{ii'}^k := \mathcal{F}_i^k - \mathcal{F}_{i'}^k, ii' \in \mathcal{E}^k$.

Node and edge feature cross-attention. To incorporate feature information across graphs, we utilize the cross attention mechanism [31]. It has been used in a number of applications like semantic correspondence [39] and point cloud registration [37] to improve feature expressivity from

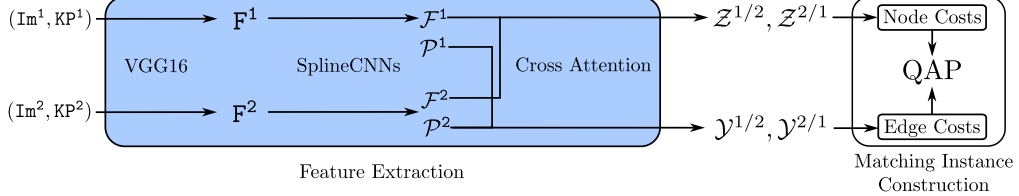


Figure 4: Information Flow Diagram for the feature processing and matching instance construction. The **feature extraction layer** is shown in the blue box. Input to the pipeline are image-keypoint pairs, $(\text{Im}^1, \text{KP}^1), (\text{Im}^2, \text{KP}^2)$ in the figure. The features extracted via a pre-trained VGG16 backbone network are refined by SplineCNN layers. The outputs of the SplineCNN layers are subsequently passed through cross-attention layers, and finally used in the construction of a matching instance.

two different sources of data. These sources can be images, point clouds or, as in our case, graphs.

Let the node features refined after the SplineCNN stage be $\mathcal{F}^k = \{\mathbf{f}_i^k \mid i \in \mathcal{V}^k\}$, $k = 1, 2$. Then the *node cross attention features for \mathcal{F}^1 with respect to \mathcal{F}^2* denoted as $\mathcal{Z}^{1/2} = \{\mathbf{z}_i^{1/2} \mid i \in \mathcal{V}^1\}$ are defined as $\mathbf{z}_i^{1/2} = \text{CA}(\mathbf{f}_i^1, \mathbf{f}^2)$. Here $\text{CA}(\mathbf{f}_i^1, \mathbf{f}^2) =$

$$\sum_{s \in \mathcal{V}_2} \text{softmax} \left(\frac{(\mathbf{f}_i^1 \mathbf{W}^Q) \cdot (\mathbf{f}_s^2 \mathbf{W}^K)^\top}{\sqrt{D}} \right) \cdot (\mathbf{f}_i^1 \mathbf{W}^T) \quad (9)$$

is the function computing the *cross-attention* between two feature vectors, \mathbf{W}^Q , \mathbf{W}^K and \mathbf{W}^T are learned projection matrices and D is the feature vector dimension. Intuitively speaking, the projection matrices learn which features to take more/less notice of.

The cross-attention node features for \mathcal{F}^2 with respect to \mathcal{F}^1 are computed analogously and denoted by $\mathcal{Z}^{2/1} = \{\mathbf{z}_s^{2/1} \mid s \in \mathcal{V}^2\}$.

Similarly we compute the *cross-attention edge features* $\mathcal{Y}^{1/2} = \{\mathbf{y}_{ij}^{1/2} \mid ij \in \mathcal{E}^1\}$ and $\mathcal{Y}^{2/1} = \{\mathbf{y}_{ij}^{2/1} \mid ij \in \mathcal{E}^2\}$ by plugging the coordinates of the edge features \mathcal{P}^1 and \mathcal{P}^2 into (9) instead of the node features \mathcal{F}^1 and \mathcal{F}^2 .

5.2. Matching instance construction

It remains to specify how the costs for the graph matching problems in Eq. (4) are computed. The unary costs c_{is} are computed as:

$$c_{is} := \left\langle \frac{\mathbf{z}_i^{1/2}}{\|\mathbf{z}_i^{1/2}\|}, \frac{\mathbf{z}_s^{2/1}}{\|\mathbf{z}_s^{2/1}\|} \right\rangle - \hat{c}. \quad (10)$$

The constant \hat{c} regulates the number of unassigned points, *i.e.*, its larger positive values decrease this number and smaller increase. We treat \hat{c} as hyper-parameter. The edge costs $c_{is,jl}$ are given by:

$$c_{is,jl} := \left\langle \frac{\mathbf{y}_{ij}^{1/2}}{\|\mathbf{y}_{ij}^{1/2}\|}, \frac{\mathbf{y}_{sl}^{2/1}}{\|\mathbf{y}_{sl}^{2/1}\|} \right\rangle. \quad (11)$$

6. Experimental validation

Compared methods. Our method termed as Cycle-Loss-based Unsupervised Graph Matching is abbreviated as CLUM. It uses the state-of-the-art QAP solver [17] at the end of the pipeline described above.

We compare our method to multiple supervised and unsupervised learning graph matching techniques.

Supervised deep graph matching methods we compare to are: GMN [41], PCA [36], NGM [35], CIE [40], BBGM [27] and NGMv2 [35].

The unsupervised methods GANN [34] and SCGM [23] described in Section 1.1 are the only existing unsupervised techniques for deep graph matching. As mentioned there, SCGM is not stand-alone and requires a supervised graph matching algorithm as a backbone. Following the original SCGM paper [23], we show results with backbones BBGM and NGMv2.

To show advantages and flexibility of our unsupervised learning framework, we test it with a different network, taken from BBGM, and another QAP solver [30], also used in BBGM. The resulting method is abbreviated as CL-BBGM. Besides the different solver, the BBGM pipeline has no attention layer and computes the matching costs differently.

Experimental setup. All experiments were run on an Nvidia-A100 GPU and a 32 core CPU. All reported results are averaged over 5 runs. The hyper-parameters are the same in all experiments. We used Adam [21] with an initial learning rate of 2×10^{-3} which is halved at regular intervals. The VGG16 backbone learning rate is multiplied by 0.01. We process batches of 12 image triplets. The hyper-parameter λ from (3) is set to 80. Hyper-parameter \hat{c} from (10) for Pascal VOC (unfiltered) is set to 0.217 for CLUM and 0.329 for CL-BBGM, respectively. Note \hat{c} is important only for the case of incomplete assignments, *i.e.*, the Pascal VOC (Unfiltered) dataset in our experiments, see below. In other experiments a sufficiently large value of \hat{c} has been used to assure complete assignments. We use image flips and rotations as augmentations. The remaining implementation details will be found in the code base which

will be made public on acceptance of the paper.

6.1. Datasets

We evaluate our proposed method on the task of keypoint matching on the following datasets: Willow Object Class [7], SPair-71K [24] and Pascal VOC with Berkeley annotations [12, 2]. All but Pascal VOC assume *complete* matching. The consolidated results are given in Table 2, while the detailed evaluation can be found in the supplement.

Following [27] all considered methods are assumed to match pairs of images of the same category with at least three keypoints in common. We apply the same rule to select the image triples for training. We will make these triples available upon acceptance.

Pascal VOC with Berkeley annotations. This dataset consists of 7,020 training images and 1,682 testing images with 20 classes in total, together with the object bounding boxes for each. Following the data preparation protocol in [36], each object within the bounding box is cropped and resized to 256×256 . Images can have up to 23 keypoints.

Following [27], we perform evaluations on the Pascal VOC dataset in two regimes:

- *Filtered*. Only the keypoints present in the matched images are preserved and all others are discarded as outliers. This regime allows to use methods restricted to complete matchings, such as NGM and CIE. For the keypoint task associated with such an *intersection filtering* we use matching accuracy to evaluate performance.
- *Unfiltered*. For a given triplet of images, the keypoints are used without any filtering. Matching instances may contain a different number of keypoints in each image, as well as outliers in all three images. This is a more general and realistic setting than intersection sampling. In this case, matching accuracy is no longer a good evaluation metric as it ignores false positives. So instead we report the F1-Score, the harmonic mean of precision and recall.

Willow object class. The benchmark [7] consists of 256 images in 5 categories, where two categories (car and motorbike) are subsets from Pascal VOC. Similar to other methods, we pre-train our method on Pascal VOC.

SPair-71K. This dataset is much larger than Pascal VOC and Willow Object. It consists of 70,958 image pairs collected from Pascal VOC 2012 and Pascal 3D+ (53,340 for training, 5,384 for validation and 12,234 for testing). It removes the ambiguous categories from Pascal VOC like sofa

and dining table. The dataset is considered to have more difficult matching instances as well as higher annotation quality.

6.2. Results

The evaluation results are summarized in Table 2 and illustrated in Table 1. For most methods we took results from the respective papers or the ThinkMatch [35] graph matching library testing webpage if available. In addition to CL-BBGM, we trained GANN on SPair-71K, as the respective results were missing in the paper. Unfortunately, the SCGM paper [23] also does not provide results for SPair-71K. In turn, we have not managed to obtain sensible results on SPair-71K and therefore do not report them. Note that *our method outperforms all its unsupervised and even some supervised competitors*. The CL-BBGM method based on our unsupervised framework also shows solid results. It is second-best on the Pascal VOC (Unfiltered) dataset assuming incomplete matching and only slightly inferior to the contrastive learning approach with the same backbone (SCGM w/BBGM) on the datasets assuming complete matching (PascalVOC (Filtered) and Willow).

We believe that using SCGM for pre-training of our method could further boost its performance. As illustrated in Table 1, the pairwise costs learned by our method not always preserve geometric constraints. Thus using SCGM as a pretext task may improve their quality.

Ablation study results are summarized in Table 3. In each experiment we change a *single* component compared to the full CLUM or CL-BBGM pipeline.

In the *CLUM – SplineCNN* experiment we remove the SplineCNN layer and set $\mathcal{F}^k := F^k$, $k = 1, 2$.

In the *CLUM – Attention* experiment we substitute the cross-attention layer by setting $\mathbf{z}^{1/2} := \mathcal{F}^1$, $\mathbf{z}^{2/1} := \mathcal{F}^2$ and $\mathbf{y}^{1/2} := \mathcal{P}^1$, $\mathbf{y}^{2/1} := \mathcal{P}^2$.

The *CL-BBGM + Attention* is the variant where our cross-attention layer is placed between the Spline-CNN and the cost computation in the CL-BBGM pipeline.

Table 3 suggests that our cross-attention layer is able to improve performance not only of CLUM, but also of the CL-BBGM pipelines. It also affirms the earlier finding that the SplineCNN is an essential component in the deep graph matching architecture when the latter is applied to keypoint matching.

Semi-supervised learning. Fig. 5 shows the result of combining our unsupervised framework with increasing amounts of ground-truth data on the Pascal VOC (Filtered) dataset. In this experiment, we randomly complement a fixed percentage of the keypoint pairs with ground-truth data. To this end these ground truth pairs are assigned very low costs to guarantee that they become a part of the optimal

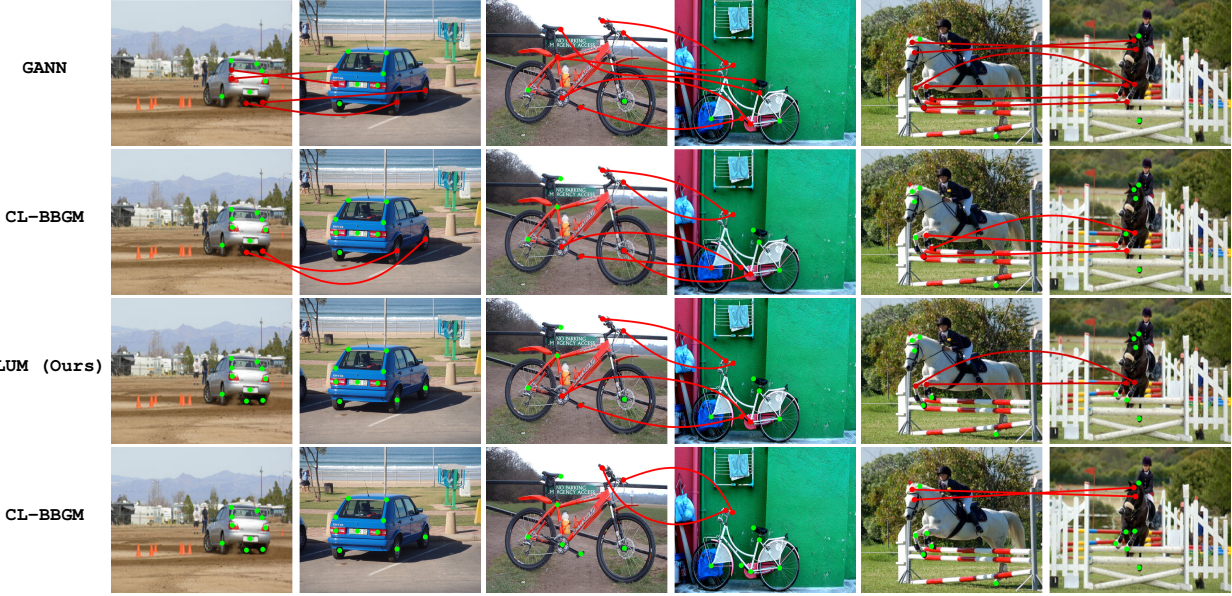


Table 1: Visualization of matching results on the SPair-71K dataset. In addition to the unsupervised techniques GANN, CL-BBGM, CLUM we show results of the fully supervised BBGM as a baseline. Correctly matched keypoints are shown as green dots, whereas incorrect matches are represented by red lines. The matched keypoints have in general similar appearance that suggests sensible unary costs. Improving of the matching quality from top to bottom is arguably mainly due to improving the pairwise costs, with the fully supervised BBGM method showing the best results.

Dataset	Metric	Supervised						Unsupervised				
		GMN	PCA	NGM	CIE	BBGM	NGMv2	GANN	SCGM w/BBGM	SCGM w/NGMv2	CL-BBGM	CLUM (Ours)
PascalVOC (Filtered)	Accuracy	55.3	64.8	64.1	68.9	79	80.1	31.5	57.1	54.3	55.3	60.1
PascalVOC (Unfiltered)	F1-Score	41.9	42.4	-	-	55.4	54.0	24.3	35.9	33.3	36.3	40.4
Willow	Accuracy	79.3	87.4	85.3	89.0	97.2	97.5	92.0	91.3	91.0	91.1	92.7
SPair-71K	Accuracy	65.3	65.9	68.9	0.7334	82.1	80.2	31.7	-	-	39.3	41.4

Table 2: Consolidated results of the various deep graph matching methods on the benchmark datasets. The best results for the supervised and unsupervised methods on each of the benchmarks are highlighted in bold.

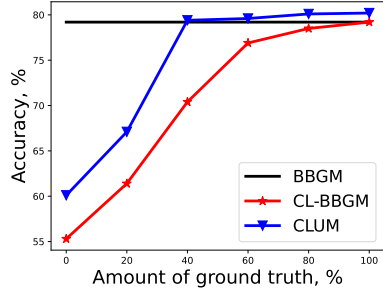


Figure 5: Semi-supervised training on Pascal VOC (Filtered). The fully supervised value of BBGM is given as a baseline.

matching. As can be seen from Fig. 5, our technique outperforms a state-of-the-art BBGM method with only 40% of the ground truth assignments. With 100% of ground truth it attains accuracy of 80.2%. This is slightly better than shown by the current fully-supervised best technique on this dataset, NGMv2, see Table 2. We expect this accuracy to improve even further if the hyper-parameters would

Ablation	Pascal VOC	SPair-71K
CLUM – Spline CNN	54.9	39.3
CLUM – Attention	58.1	40.4
CL-BBGM + Attention	58.7	40.9
CL-BBGM	55.3	39.3
CLUM	60.1	41.4

Table 3: The ablation study on the Pascal VOC (filtered) and SPair-71K datasets. Numbers show accuracy in percents. be tuned for the fully supervised mode. As expected, the performance of CL-BBGM gradually converges to those of BBGM as the amount of labelled data increases.

7. Conclusions

We presented a new framework for unsupervised cycle-loss-based training of deep graph matching. It is extremely flexible in terms of the neural networks, as well as combinatorial solvers it can be used with. Filled with the best components it outperforms state-of-the art and its flexibility suggests that its performance improves with the improve-

ment of the components.

We believe that our framework can be adapted also to other keypoint-based deep learning pipelines like 6D pose estimation, object tracking, keypoint discovery and correspondence estimation.

8. Acknowledgements

We thank the Center for Information Services and High Performance Computing (ZIH) at TU Dresden for its facilities for high throughput calculations. Bogdan Savchynskyy was supported by the German Research Foundation (project number 498181230).

References

- [1] Peter W. Battaglia, Jessica B. Hamrick, Victor Bapst, Alvaro Sanchez-Gonzalez, Vinicius Flores Zambaldi, Mateusz Malinowski, Andrea Tacchetti, David Raposo, Adam Santoro, Ryan Faulkner, Çaglar Gülcöhre, H. Francis Song, Andrew J. Ballard, Justin Gilmer, George E. Dahl, Ashish Vaswani, Kelsey R. Allen, Charles Nash, Victoria Langston, Chris Dyer, Nicolas Heess, Daan Wierstra, Pushmeet Kohli, Matthew M. Botvinick, Oriol Vinyals, Yujia Li, and Razvan Pascanu. Relational inductive biases, deep learning, and graph networks. *CoRR*, abs/1806.01261, 2018. [1](#)
- [2] Lubomir Bourdev and Jitendra Malik. Poselets: Body part detectors trained using 3d human pose annotations. In *2009 IEEE 12th International Conference on Computer Vision*, pages 1365–1372. IEEE, 2009. [7](#)
- [3] Lev M Bregman. The relaxation method of finding the common point of convex sets and its application to the solution of problems in convex programming. *USSR Computational Mathematics and Mathematical Physics*, 1967. [2](#)
- [4] William Brendel and Sinisa Todorovic. Learning spatiotemporal graphs of human activities. In *2011 International Conference on Computer Vision*, pages 778–785. IEEE, 2011. [1](#)
- [5] Rainer Burkard, Mauro Dell’Amico, and Silvano Martello. *Assignment problems: revised reprint*. SIAM, 2012. [2](#)
- [6] Dongliang Cao and Florian Bernard. Unsupervised deep multi-shape matching. In *European Conference on Computer Vision*, pages 55–71. Springer, 2022. [3](#)
- [7] Minsu Cho, Karteek Alahari, and Jean Ponce. Learning graphs to match. In *Proceedings of the IEEE International Conference on Computer Vision*, pages 25–32, 2013. [7](#)
- [8] David F Crouse. On implementing 2D rectangular assignment algorithms. *IEEE Transactions on Aerospace and Electronic Systems*, 52(4):1679–1696, 2016. [2](#)
- [9] Boris Delaunay. Sur la sphère vide. A la mémoire de georges vorono. *Bulletin de l’Académie des Sciences de l’URSS. Classe des sciences mathématiques et naturelles*, 6:793, 1934. [5](#)
- [10] Jia Deng, Wei Dong, Richard Socher, Li-Jia Li, Kai Li, and Li Fei-Fei. Imagenet: A large-scale hierarchical image database. In *2009 IEEE conference on computer vision and pattern recognition*, pages 248–255. Ieee, 2009. [5](#)
- [11] Marvin Eisenberger, Aysim Toker, Laura Leal-Taixé, Florian Bernard, and Daniel Cremers. A unified framework for implicit Sinkhorn differentiation. In *Proceedings of the IEEE/CVF Conference on Computer Vision and Pattern Recognition*, pages 509–518, 2022. [2](#)
- [12] Mark Everingham, Luc Van Gool, Christopher KI Williams, John Winn, and Andrew Zisserman. The Pascal visual object classes (VOC) challenge. *International journal of computer vision*, 88(2):303–338, 2010. [7](#)
- [13] Matthias Fey, Jan Eric Lenssen, Christopher Morris, Jonathan Masci, and Nils M. Kriege. Deep graph matching consensus. In *8th International Conference on Learning Representations, ICLR*, 2020. [2, 5](#)
- [14] Matthias Fey, Jan Eric Lenssen, Frank Weichert, and Heinrich Müller. SplineCNN: Fast geometric deep learning with continuous b-spline kernels. In *Proceedings of the IEEE conference on computer vision and pattern recognition*, pages 869–877, 2018. [5](#)
- [15] Kexue Fu, Shaolei Liu, Xiaoyuan Luo, and Manning Wang. Robust point cloud registration framework based on deep graph matching. In *Proceedings of the IEEE/CVF Conference on Computer Vision and Pattern Recognition*, pages 8893–8902, 2021. [1](#)
- [16] Stefan Haller, Lorenz Feineis, Lisa Hutschenreiter, Florian Bernard, Carsten Rother, Dagmar Kainmüller, Paul Swo-boda, and Bogdan Savchynskyy. A comparative study of graph matching algorithms in computer vision. In *European Conference on Computer Vision*, pages 636–653. Springer, 2022. [2, 4](#)
- [17] Lisa Hutschenreiter, Stefan Haller, Lorenz Feineis, Carsten Rother, Dagmar Kainmüller, and Bogdan Savchynskyy. Fusion moves for graph matching. In *Proceedings of the IEEE/CVF International Conference on Computer Vision*, pages 6270–6279, 2021. [4, 6](#)
- [18] Bo Jiang, Pengfei Sun, and Bin Luo. Glmnet: Graph learning-matching networks for feature matching. 2022. [2](#)
- [19] Andrew Zisserman Karen Simonyan. Very deep convolutional networks for large-scale image recognition. In *International Conference on Learning Representations, ICLR*, 2015. [2, 5](#)
- [20] Seungryong Kim, Dongbo Min, Bumsub Ham, Sangryul Jeon, Stephen Lin, and Kwanghoon Sohn. FCSS: Fully convolutional self-similarity for dense semantic correspondence. In *Proceedings of the IEEE Conference on Computer Vision and Pattern Recognition*, pages 6560–6569, 2017. [2](#)
- [21] Diederik P. Kingma and Jimmy Ba. Adam: A method for stochastic optimization. In Yoshua Bengio and Yann LeCun, editors, *3rd International Conference on Learning Representations, ICLR 2015*, 2015. [6](#)
- [22] Qinsong Li, Shengjun Liu, Ling Hu, and Xinru Liu. Shape correspondence using anisotropic Chebyshev spectral CNNs. In *Proceedings of the IEEE/CVF Conference on Computer Vision and Pattern Recognition*, pages 14658–14667, 2020. [5](#)
- [23] Chang Liu, Shaofeng Zhang, Xiaokang Yang, and Junchi Yan. Self-supervised learning of visual graph matching. In *European Conference on Computer Vision*, pages 370–388. Springer, 2022. [2, 6, 7](#)

[24] Juhong Min, Jongmin Lee, Jean Ponce, and Minsu Cho. Spair-71k: A large-scale benchmark for semantic correspondence. *arXiv preprint arXiv:1908.10543*, 2019. 7

[25] Alex Nowak, Soledad Villar, Afonso S Bandeira, and Joan Bruna. Revised note on learning quadratic assignment with graph neural networks. In *2018 IEEE Data Science Workshop (DSW)*, pages 1–5. IEEE, 2018. 2

[26] Gabriel Peyré and Marco Cuturi. Computational optimal transport. *Center for Research in Economics and Statistics Working Papers*, (2017-86), 2017. 2

[27] Michal Rolínek, Paul Swoboda, Dominik Zietlow, Anselm Paulus, Vít Musil, and Georg Martius. Deep graph matching via blackbox differentiation of combinatorial solvers. In *European Conference on Computer Vision*, pages 407–424. Springer, 2020. 2, 4, 5, 6, 7

[28] Yusuf Sahillioglu. Recent advances in shape correspondence. *The Visual Computer*, 36(8):1705–1721, 2020. 1

[29] Paul Swoboda, Dagmar Kainmüller, Ashkan Mokarian, Christian Theobalt, and Florian Bernard. A convex relaxation for multi-graph matching. In *Proceedings of the IEEE/CVF Conference on Computer Vision and Pattern Recognition*, pages 11156–11165, 2019. 2, 4

[30] Paul Swoboda, Carsten Rother, Hassan Abu Alhaija, Dagmar Kainmüller, and Bogdan Savchynskyy. A study of Lagrangean decompositions and dual ascent solvers for graph matching. In *Proceedings of the IEEE Conference on Computer Vision and Pattern Recognition*, 2017. 6

[31] Ashish Vaswani, Noam Shazeer, Niki Parmar, Jakob Uszkoreit, Llion Jones, Aidan N Gomez, Łukasz Kaiser, and Illia Polosukhin. Attention is all you need. *Advances in neural information processing systems*, 30, 2017. 5

[32] Nitika Verma, Adnane Boukhayma, Edmond Boyer, and Jakob Verbeek. Dual mesh convolutional networks for human shape correspondence. In *2021 International Conference on 3D Vision (3DV)*, pages 289–298. IEEE, 2021. 5

[33] Marin Pogančić Vlastelica, Anselm Paulus, Vit Musil, Georg Martius, and Michal Rolínek. Differentiation of blackbox combinatorial solvers. In *International Conference on Learning Representations*, 2019. 1, 2, 3

[34] Runzhong Wang, Junchi Yan, and Xiaokang Yang. Graduated assignment for joint multi-graph matching and clustering with application to unsupervised graph matching network learning. *Advances in Neural Information Processing Systems*, 33:19908–19919, 2020. 2, 6

[35] Runzhong Wang, Junchi Yan, and Xiaokang Yang. Neural graph matching network: Learning Lawler’s quadratic assignment problem with extension to hypergraph and multiple-graph matching. *IEEE Transactions on Pattern Analysis and Machine Intelligence*, 2021. 2, 6, 7, 12

[36] Xiaolong Wang, Allan Jabri, and Alexei A Efros. Learning correspondence from the cycle-consistency of time. In *Proceedings of the IEEE/CVF Conference on Computer Vision and Pattern Recognition*, pages 2566–2576, 2019. 2, 5, 6, 7

[37] Yue Wang and Justin M Solomon. Deep closest point: Learning representations for point cloud registration. In *Proceedings of the IEEE/CVF International Conference on Computer Vision*, pages 3523–3532, 2019. 5

[38] Junchi Yan, Chao Zhang, Hongyuan Zha, Wei Liu, Xiaokang Yang, and Stephen M Chu. Discrete hyper-graph matching. In *Proceedings of the IEEE conference on computer vision and pattern recognition*, pages 1520–1528, 2015. 11

[39] Hao Yu, Fu Li, Mahdi Saleh, Benjamin Busam, and Slobodan Ilic. Cofinet: Reliable coarse-to-fine correspondences for robust pointcloud registration. *Advances in Neural Information Processing Systems*, 34:23872–23884, 2021. 5

[40] Tianshu Yu, Runzhong Wang, Junchi Yan, and Baoxin Li. Learning deep graph matching with channel-independent embedding and Hungarian attention. In *International conference on learning representations*, 2019. 2, 6

[41] Andrei Zanfir and Cristian Sminchisescu. Deep learning of graph matching. In *Proceedings of the IEEE conference on computer vision and pattern recognition*, pages 2684–2693, 2018. 2, 6

[42] Jiawei Zhang and S Yu Philip. Multiple anonymized social networks alignment. In *2015 IEEE International Conference on Data Mining*, pages 599–608. IEEE, 2015. 1

[43] Tinghui Zhou, Philipp Krahenbuhl, Mathieu Aubry, Qixing Huang, and Alexei A Efros. Learning dense correspondence via 3d-guided cycle consistency. In *Proceedings of the IEEE Conference on Computer Vision and Pattern Recognition*, pages 117–126, 2016. 2

A. Supplementary

Detailed Results for the Object Classes for the Benchmark Datasets

A.1. PascalVOC

Type	Method	aero	bike	bird	boat	bottle	bus	car	cat	chair	cow	table	dog	horse	motor	person	plant	sheep	sofa	train	TV	Mean
Supervised	GMM	31.9	47.2	51.9	40.8	68.7	72.2	53.6	52.8	34.6	48.6	72.3	47.7	54.8	51.0	38.6	75.1	49.5	45.0	83.0	86.0	55.3
	PCA	49.8	61.9	65.3	57.2	78.8	75.6	64.7	69.7	41.6	63.4	50.7	67.1	66.7	61.6	44.5	81.2	67.8	59.2	78.5	90.4	64.8
	NGM	50.1	63.5	57.9	53.4	79.8	77.1	73.6	68.2	41.1	66.4	40.8	60.3	61.9	63.5	45.6	77.1	69.3	65.5	79.2	88.2	64.1
	CIE	52.5	68.6	70.2	57.1	82.1	77.0	70.7	73.1	43.8	69.9	62.4	70.2	70.3	66.4	47.6	85.3	71.7	64.0	83.8	91.7	68.9
	BB-GM	61.9	71.1	79.7	79.0	87.4	94.0	89.5	80.2	56.8	79.1	64.6	78.9	76.2	75.1	65.2	98.2	77.3	77.0	94.9	93.9	79
	NGMv2	61.8	71.2	77.6	78.8	87.3	93.6	87.7	79.8	55.4	77.8	89.5	78.8	80.1	79.2	62.6	97.7	77.7	75.7	96.7	93.2	80.1
Unsupervised	GANN	19.2	20.5	24.1	27.9	30.8	50.9	36.4	22.3	24.4	23.2	39.8	21.7	20.5	23.9	15.8	42.2	29.8	17.1	61.8	78.0	31.5
	SCGM w/BBGM	37.6	49.9	54.8	54.5	65.6	56.4	60.6	52.3	36.8	51.4	50.4	47.2	59.4	51.2	38.3	91.3	59.3	52.7	83.1	88.4	57.1
	SCGM w/NGMv2	34.3	48.2	51.0	52.2	63.3	56.0	62.0	50.1	38.5	49.9	39.9	46.2	54.8	52.1	37.4	82.3	56.8	51.4	80.2	78.8	54.3
	CL-BBGM	38.3	51.4	57.7	53.1	67.4	54.9	62.3	51.4	35.1	52.1	51.0	45.7	60.3	52.4	39.3	83.7	61.4	53.5	81.9	81.4	55.3
	CLUM (Ours)	40.4	51.6	56.7	52.5	69.7	57.8	63.3	51.9	38.0	54.4	53.1	47.6	62.2	52.1	43.3	85.6	60.5	60.4	82.9	86.6	60.1

Table 4: Accuracy (%) on Pascal VOC with standard intersection filtering. The methods are grouped by labelled, and unlabelled learning from top to bottom (see “Type”).

Type	Method	aero	bike	bird	boat	bottle	bus	car	cat	chair	cow	table	dog	horse	motor	person	plant	sheep	sofa	train	TV	Mean
Supervised	GMM	28.0	55.0	33.1	27.0	79.0	52.0	26.0	40.2	28.4	36.0	29.8	33.7	39.4	43.0	22.1	71.8	30.8	25.9	58.8	78.0	41.9
	PCA	27.5	56.5	36.6	27.7	77.8	49.2	23.9	42.3	27.4	38.2	38.7	36.5	39.3	42.8	25.6	74.3	32.6	24.7	51.5	74.3	42.4
	BB-GM	37.0	65.0	50.1	34.8	86.7	67.1	25.4	56.1	41.6	58.0	38.3	52.9	55.0	66.6	30.7	96.5	49.5	36.4	76.4	83.1	55.4
	NGMv2	39.4	66.1	49.6	41.0	87.9	59.6	46.3	52.9	39.5	53.1	31.0	49.7	51.0	60.3	42.2	91.5	41.3	37.1	65.7	74.8	54.0
	GANN	12.6	19.5	16.6	18.5	41.1	32.4	19.3	12.3	24.3	17.2	38.0	12.2	15.9	18.2	19.4	35.5	14.8	15.4	41.5	60.8	24.3
	SCGM w/BBGM	18.9	43.5	32.3	29.5	64.4	36.1	20.3	28.8	23.9	28.8	23.7	23.3	31.4	33.4	21.1	83.2	25.5	27.0	49.4	72.9	35.9
Unsupervised	SCGM w/NGMv2	19.7	42.2	29.5	23.9	62.3	35.2	21.2	27.3	24.1	25.9	22.8	23.5	30.3	35.7	21.3	67.5	24.6	21.6	44.4	65.6	33.3
	CL-BBGM	21.4	43.8	29.5	23.9	61.7	37.8	21.9	30.2	23.5	29.1	28.7	22.7	29.7	32.7	19.3	77.8	25.8	28.6	50.4	67.6	36.3
	CLUM (Ours)	23.2	44.2	30.5	29.7	63.7	40.1	21.6	31.4	22.7	31.4	39.4	23.8	33.9	34.4	19.7	84.1	27.3	31.1	51.1	69.0	40.4

Table 5: F1 score (%) (the higher the better) on Pascal VOC without filtering. It denotes that all graphs can contain outliers. The methods are grouped by labelled and unlabelled (see “Type”). The methods NGM and CIE are not shown as their do not support incomplete matchings.

A.2. Willow Object Class

Type	Method	Car	Duck	Face	Motorbike	Winebottle	Mean
Supervised	GMM [38]	67.9	76.7	99.8	69.2	83.1	79.3
	PCA	87.6	83.6	100.0	77.6	88.4	87.4
	NGM	84.2	77.6	99.4	76.8	88.3	85.3
	CIE	85.8	82.1	99.9	88.4	88.7	89.0
	BBGM	96.8	89.9	100.0	99.8	99.4	97.2
	NGM v2	97.4	93.4	100.0	98.6	98.3	97.5
Unsupervised	GANN	85.4	89.8	100.0	88.6	96.4	92.0
	SCGM w/ BBGM	91.3	73.0	100.0	95.6	96.6	91.3
	SCGM w/ NGM v2	91.2	74.4	99.7	96.8	92.7	91.0
	CL-BBGM	91.1	88.4	100.0	92.6	95.6	91.1
	CLUM (Ours)	91.3	93.4	100.0	96.6	98.6	92.7

Table 6: Mean accuracy (%) across all the objects in the Willow Object dataset. The methods are grouped by supervised learning and self-supervised learning. Please note that SCGM is trained on the Pascal VOC dataset and finetuned on Willow Object.

A.3. SPair-71K

Type	Method	aero	bicycle	chicken	boat	bottle	bus	car	cat	chair	cow	dot	horse	motor	person	plant	sheep	train	TV	Mean
Supervised	GMN	60.9	51.0	74.3	46.72	63.3	75.5	69.5	64.6	57.5	73.0	58.7	59.1	63.2	51.2	86.9	57.9	70.0	92.4	65.3
	PCA	64.7	45.7	78.1	51.3	63.8	72.7	61.2	62.8	62.6	68.2	59.1	61.2	64.9	57.8	87.4	60.4	72.5	92.8	65.9
	NGM	66.4	52.6	76.9	49.6	67.6	78.8	67.6	68.3	59.2	73.6	63.9	60.7	70.7	60.9	87.5	63.9	79.8	91.5	68.9
	BB-GM	72.5	64.6	87.8	75.8	69.3	93.9	88.6	79.9	74.6	83.2	78.8	77.1	76.5	76.3	98.2	85.5	96.8	99.3	82.1
	NGMv2	68.8	63.3	86.8	70.1	69.7	94.7	87.4	77.4	72.1	80.7	74.3	72.5	79.5	73.4	98.9	81.2	94.3	98.7	80.2
Unsupervised	GANN	27.8	22.4	41.8	19.5	37.1	49.8	24.5	15.9	24.2	38.7	23.9	17.3	29.3	17.6	40.3	19.9	56.6	64.9	31.7
	CL-BBGM	29.3	24.3	44.5	22.5	38.4	46.7	30.1	28.3	28.9	39.0	34.3	55.6	25.1	45.4	53.1	29.6	73.4	59.1	39.3
	Ours (CLGM)	30.4	25.7	46.0	24.8	38.9	48.7	30.9	28.0	31.4	41.5	37.5	59.3	27.8	43.9	57.2	32.3	75.8	62.7	41.4

Table 7: Keypoint matching accuracy (%) on SPair-71k for all classes. The results for the supervised methods are taken from the ThinkMatch [35] graph matching library webpage.